

# Urban Air Pollution by Laser Photoacoustic Spectroscopy and Simplified Numerical Modeling of Gas Pollution in Urban Canyon

MIOARA PETRUS<sup>1</sup>, CRISTINA POPA<sup>1</sup>, ANA-MARIA BRATU<sup>1</sup>

<sup>1</sup>Laser Department,

National Institute for Laser, Plasma, and Radiation Physics,  
409 Atomistilor St., PO Box MG 36, 077125 Magurele, Ilfov,  
ROMANIA

*Abstract:* - With rapid urbanization and industrialization, atmospheric pollution has emerged as a significant environmental challenge in Romania. Employing a laser photoacoustic spectroscopy detector, researchers analyzed ethylene, benzene, and toluene simultaneously across three distinct environmental settings in the country's southern region. This investigation spanned from March to August 2021, covering both spring and summer seasons. Measurements were taken at a breathing height of 1.5 meters above ground level. The highest concentrations of ethylene ( $116.82 \pm 82.37$  ppb), benzene ( $1.13 \pm 0.32$  ppb), and toluene ( $5.48 \pm 3.27$  ppb) were recorded at measurement point P1, situated within the city amidst residential buildings during the summer season. Additionally, the highest ozone levels ( $154.75 \pm 68.02$  ppb) were observed at point P3, located in an industrial area, during the summer. The behavior of gas concentrations is influenced by meteorological factors such as temperature, wind speed, and direction. The high toluene/benzene ratio suggests that traffic and industrial emissions are the primary sources of these pollutants. Notably, benzene and ozone concentrations exceeded prescribed limit values based on the measurements. Concurrently, a numerical model was employed to assess the impact of greenery on mitigating pollution in urban canyons. Specifically, the study focused on how wind velocity affects the dispersion of benzene pollutants in a street canyon. This study's governing equations utilized for air pollutant flow were the Reynolds-averaged Navier–Stokes (RANS) equations for compressible turbulent flow and moisture transport in air, implemented through Comsol software.

*Key-Words:* - laser photoacoustic spectroscopy, air pollution, ethylene, benzene, toluene, numerical simulation.

Received: February 16, 2023. Revised: December 19, 2023. Accepted: February 15, 2024. Published: April 10, 2024.

## 1 Introduction

Clean air is essential for all life forms on Earth. Not only does air quality impact human health, but it also affects crucial environmental components such as water, soil, and forests, which are vital resources for human development, [1]. Urbanization, characterized by a relative increase in a country's urban population alongside a faster growth in the economic, political, and cultural significance of cities compared to rural areas, is an integral aspect of economic development, [1]. However, urbanization brings various challenges, including the rise in urban population, high population density, expansion of industrial activities (both medium and small scale within urban areas and large scale in surrounding areas), the proliferation of high-rise buildings, and increased vehicular traffic, [2]. These activities collectively contribute to air pollution. The configuration of a city and the distribution of land use determine the placement of emission sources and the flow of urban traffic, which significantly impacts urban air quality.

Factors such as geographical location, climate, meteorological conditions, city planning and design, and human activities play crucial roles in the dispersion and distribution of air pollutants, thereby influencing urban air quality, [3].

## 2 Problem Formulation

Various types of pollution, including air, water, thermal, noise, and soil contamination, present significant environmental challenges. Among these, air pollution stands out as the primary cause of mortality globally, with reports indicating millions of lives lost due to pollution-related causes, [4]. Key air pollutants mainly stem from industrial activities, factories, and transportation sources, such as carbon dioxide, volatile organic compounds (VOCs), nitrogen dioxide, ozone particles, and sulfur dioxide. In urban areas, vehicle emissions notably contribute to air pollution, particularly in densely populated centers, placing a significant burden on the transportation sector, [5].

Given the adverse effects of air pollution on public health, it is crucial to understand how to maintain acceptable air quality levels, particularly in urban settings like street canyons. Implementing strategies to mitigate air pollution in these areas is essential for safeguarding public health and promoting environmental well-being, [6].

Despite advancements in providing information on air quality, there remains a critical need for national-level studies on air quality, which serves as the primary motivation for this research. This study aims to passively quantify ambient air concentrations of ethylene ( $C_2H_4$ ), benzene ( $C_6H_6$ ), and toluene ( $C_7H_8$ ) at a breathing level of 1.5 meters above ground using a multi-component laser photoacoustic spectroscopy detector. Additionally, the research seeks to examine data related to environmental factors and meteorological variables. Our analysis focuses on investigating the influence of temperature, wind speed, and direction on ozone concentrations, as well as identifying daily and seasonal patterns and differences in environmental structural architecture.

### 3 Problem Solution

Passive measurements of ozone concentration were conducted utilizing a laser-based photoacoustic spectroscopy (LPAS) system. This advanced technique is renowned for its high sensitivity, capable of detecting gas molecules at the parts per billion (ppb) level. LPAS offers numerous advantages, including high accuracy and selectivity, a wide dynamic range, and the capability to analyze multiple components simultaneously, [7]. The diagram of the photoacoustic detector (PA) utilized for determining ozone concentration in ambient air is illustrated in Figure 1. This system comprises a  $CO_2$  laser, a PA cell, the detection unit, and a vacuum/gas handling system. The  $CO_2$  laser utilized in this setup is a frequency-stabilized laser source emitting in continuous wave (cw) across 57 different lines within the range of  $9.2 - 10.8 \mu m$ . This range is further divided into 4 branches: 9R, 9P, 10R, and 10P. The continuous-wave, tunable  $CO_2$  laser beam is subjected to chopping, focused by a ZnSe lens, and then directed into the photoacoustic cell (PA). Inside the PA cell, the laser beam's power is measured using a laser radiometer, specifically the Rk-5700 model from Laser Probe Inc., with a measuring head designated as RkT-30. The digital output from this measurement is integrated into the data acquisition interface module alongside the output from the lock-in amplifier.

Experimental data are subsequently processed and stored using a computer.

The light beam is modulated using a high-quality mechanical chopper, specifically the DigiRad C-980 or C-995 models (30-slot aperture), known for low vibration noise and variable speed capabilities ranging from 4 to 4000 Hz. Importantly, the chopper operates at the resonant frequency of the cell, set at 564 Hz. Acoustic waves generated within the cell are captured by microphones strategically positioned in the cell wall. These microphone signals are then directed to a lock-in amplifier synchronized with the modulation frequency. The lock-in amplifier serves as a versatile signal recovery and analysis tool, capable of accurately measuring a single-frequency signal even in the presence of noise sources thousands of times its magnitude. Notably, it effectively filters out random noise, transients, incoherent discrete frequency interference, and harmonics of the measurement frequency.

A dual-phase, digital lock-in amplifier is employed, specifically the Stanford Research Systems model SR 830, which offers full-scale sensitivity ranging from 2 nV to 1 V; input noise at 6 nV (rms)/ Hz at 1 kHz; dynamic reserve exceeding 100 dB; a broad frequency range spanning from 1 mHz to 102 kHz; and flexible time constants ranging from 10  $\mu s$  to 30 s (for reference frequencies  $> 200$  Hz) or extending up to 30,000 s (for reference frequencies  $< 200$  Hz).

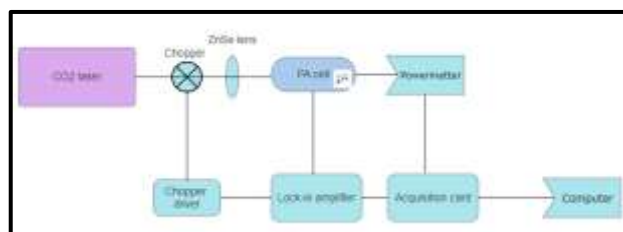


Fig. 1: A schematic representation of the LPAS system employed for determining the ambient air pollutant concentrations

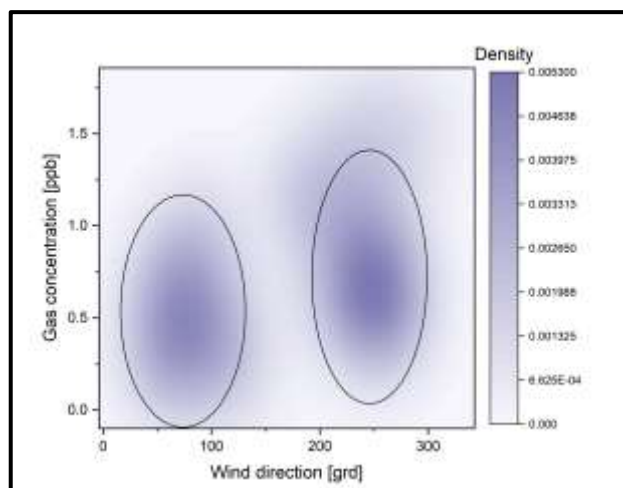
This research initiative forms part of a broader campaign aimed at determining the concentrations of various pollutants in the atmosphere utilizing a multicomponent detector based on laser photoacoustic spectroscopy, [8]. Specifically, monitoring of tropospheric ozone levels was conducted in the town of Magurele (located at  $44^{\circ}20'58''N$ ,  $26^{\circ}01'47''E$ , with an altitude of 93 meters) in Romania. This monitoring took place from March to August 2021, spanning the spring and summer seasons. Atmospheric air sampling was conducted at three distinct locations in Magurele:

P1: Latitude 44°21'02.7"N, Longitude 26°01'42.0"E. This point is situated within the city, amidst residential buildings and adjacent to a traffic roundabout. It is approximately 150 meters away from a school with over 1000 students and a kindergarten accommodating over 300 children aged 3 to 6 years. P2: Latitude 44°21'10.4"N, Longitude 26°02'31.0"E. Positioned in a small forest area dominated by oak (*Quercus robur*) and acacia (*Robinia pseudoacacia*) trees, P2 is bordered by two heavily trafficked roads, one of which is the Bucharest beltway. P3: Latitude 44°22'09.6"N, Longitude 26°02'34.2"E. Located in an industrial area, P3 is characterized by heavy vehicular traffic, including cars, gas stations, and a concrete station. Greenery is notably absent in this vicinity.

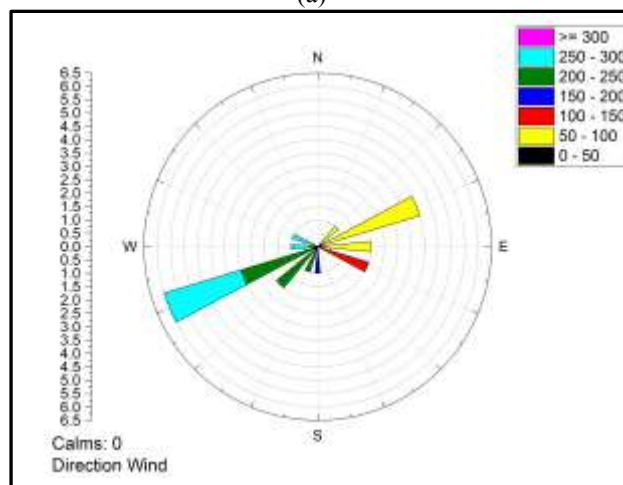
Ambient air samples were gathered at a height of 1.5 meters above the ground using specialized containers or bags. Sampling activities were conducted exclusively on working days, from Monday to Friday, within a designated time frame spanning from 8:30 am to 8:30 pm. At each sampling location, a total of six samples were collected: three during the morning period from 8:30 to 11:30 am, and three during the evening period from 5:30 to 8:30 pm. This sampling strategy was designed to provide a comprehensive representation of environmental conditions at various times of the day, enabling a more thorough analysis of variations in trace gases or other pertinent parameters over the day. By incorporating dual sampling timeframes, the study aimed to capture potential diurnal fluctuations, ensuring a robust understanding of the environmental characteristics at each specific location. The mean week value of concentrations of ethylene, benzene, and toluene in the three locations during the spring and summer seasons are presented in Table 1.

Table 1. Ethylene, benzene, and toluene mean± SD in P1, P2, and P3 points in the spring and summer seasons

VOCs	Spring Concentration ± SD [ppb]			Summer Concentration ± SD [ppb]		
	P1	P2	P3	P1	P2	P3
C <sub>2</sub> H <sub>4</sub>	56.14 ±21.49	58.34 ±25.06	55.76 ±31.61	116.86 ±82.37	104.28 ±41.17	87.23 ±46.43
C <sub>6</sub> H <sub>6</sub>	0.62 ±0.32	0.35± 0.17	0.57± 0.21	1.13 ± 0.32	0.624 ± 0.19	0.98 ±0.26
C <sub>7</sub> H <sub>8</sub>	1.99 ± 0.84	1.49 ± 0.73	1.80 ± 0.88	5.48 ± 3.27	4.32 ± 3.07	5.26 ± 3.11



(a)



(b)

Fig. 2: (b) Distribution of the VOC concentrations in the three measurement locations according to the wind direction in the March-August 2021 period; (b) Wind rose in Magurele from March to August 2021

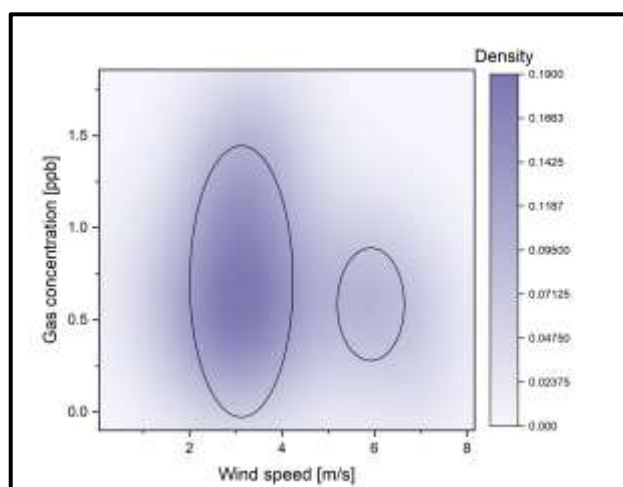


Fig. 3: The distribution of the VOC concentrations in the three measurement locations according to the wind speed in the March–August 2021 period

Figure 2 illustrates the distribution of ozone concentrations at measuring points P1, P2, and P3 relative to wind direction. The data suggests a correlation between ozone levels and wind direction, with lower ozone concentrations observed when the wind originates from the east (E) or northeast (NE) direction (54 - 91.5 degrees), and higher ozone levels recorded when the wind blows from the south (S) or southwest (SV) direction (180 - 273.9 degrees). In Figure 3, the distribution of ozone concentrations at points P1, P2, and P3 is depicted as a function of wind speed. Notably, a significant portion of ozone concentrations appears to fall within the range of 2.5 - 4 meters per second (m/s) wind speeds.

Elevated levels of ethylene, benzene, and toluene were observed in association with southwest and northeast wind directions, particularly at wind speeds ranging between 2-4 m/s and 6-7 m/s. Various studies have investigated the influence of wind direction and speed on urban air quality, including its impact on gaseous pollutants, [9]. Notably, higher wind speeds have been linked to a decrease in air pollutant concentrations. Wind direction plays a critical role in determining the flow patterns and dispersion of pollutants within a given area. For instance, in elongated street canyons, wind direction influences airflow and the distribution of pollutants, resulting in differing concentrations on leeward and windward-facing walls. Additionally, factors such as street size and geometry contribute, with irregular streets potentially restricting pollutant dispersion and exposing nearby residents to higher concentrations of pollutants, [10], [11].

The toluene/benzene (T/B) ratio serves as a valuable indicator for discerning the sources of VOCs, particularly aromatics, [12]. Different sources exhibit distinct T/B ratio ranges: i) Vehicle Emissions: In areas heavily impacted by vehicle emissions, the T/B ratio typically falls within the range of 0.9–2.2. ii) Solvent Use: Higher T/B ratios, exceeding 8.8, are commonly reported for activities involving solvent use. iii) Industrial Processes: T/B ratios ranging from 1.4 to 5.8 have been observed in industrial settings, indicating emissions from various industrial processes. iv) Burning Source Emissions: Studies focusing on emissions from burning sources, including combustion processes and raw materials, have reported T/B ratios below 0.6. By analyzing the T/B ratio in ambient air samples, researchers can gain insights into the predominant sources of aromatic compounds present in a specific environment. Table 2 presents the T/B ratio values obtained in this study. This implies that the atmospheric occurrence of benzene

and toluene in the measurement areas can be attributed to emissions from both traffic and industrial sources.

Table 2. The values of T/B ratio

Location	Spring			Summer		
	P1	P2	P3	P1	P2	P3
T/B ratio value	3.21	4.26	3.16	4.85	6.92	5.37

## 4 Numerical Simulation

Turbulence presents a longstanding challenge in classical physics, demanding resolution due to its prevalence in natural phenomena and various technological processes. The significance of this problem stems from the fact that the majority of flows observed in nature and industrial applications exhibit turbulent characteristics. To tackle turbulence mathematically, several approaches have been developed. Among these, the Reynolds approach is the most prevalent. This approach leads to the derivation of a Reynolds-averaged Navier–Stokes system of equations (RANS), which serves as a fundamental framework for understanding and modeling turbulent flow behavior, [13].

Although RANS methods are widely employed, certain hydrodynamic problems may not yield satisfactory results, necessitating high computational cell resolution. COMSOL Multiphysics is a robust software package used for modeling physical phenomena across various disciplines, including fluid dynamics and chemical reactions. It employs the Finite Element Method to solve hydrodynamic equations. In addressing aerodynamic profile problems, the initial distribution of velocity and pressure is determined by the potential field of velocities. The velocity potential must adhere to the continuity equation for incompressible flow. Following the calculation of the velocity potential, pressure can be approximated using the Bernoulli equation. The k-ε turbulence model stands out as one of the most common models utilized in CFD to simulate mean flow characteristics under turbulent flow conditions, [13], [14].

To depict the transport of C<sub>6</sub>H<sub>6</sub> within a street canyon using Comsol, a transport model was formulated for the system. In the context of a single-pollutant approach focusing on C<sub>6</sub>H<sub>6</sub>, the governing equations for the problem during an adiabatic process are the RANS equations. In the numerical simulation, identical dimensions were employed for the city corridor as those at the P1 measurement point. Benzene was selected as the pollutant due to its severe impact on human health, being classified

as a Class 1 human carcinogen. The size of the geometry used in the numerical simulation was: L (length) = 165 m, l (width) = 72 m, h (height of the buildings) = 17 m. On the street segment used, there are several 7 residential buildings 3 floors each. The parameters of benzene used in the simulation are presented in Table 3.

Table 3. Benzene parameters used in numerical simulation

Parameter	Value
Density [kg/m <sup>3</sup> ]	3.486
Dynamic viscosity [Pa*s]	569.8e <sup>-6</sup>
Temperature [K]	303.15

Initially, a mesh independence analysis was conducted for the three geometries under consideration. The selected criterion aimed to strike a reasonable balance between accuracy and computational efficiency. Consequently, for the final simulations, the mesh ensuring that the average concentration on the outlet surface remained within a confidence range lower than 4% was adopted. A structured mesh composed of hexahedral elements was employed in the final computations for the urban canyon. In the numerical simulation, identical experimental parameters for benzene in the urban canyon were utilized, with a wind inlet velocity of 0.5 m/s. Figure 4 shows the mesh of the urban canyon geometry, Figure 5 shows the benzene gas flow velocity, and Figure 6 shows the pressure distribution in the urban canyon.

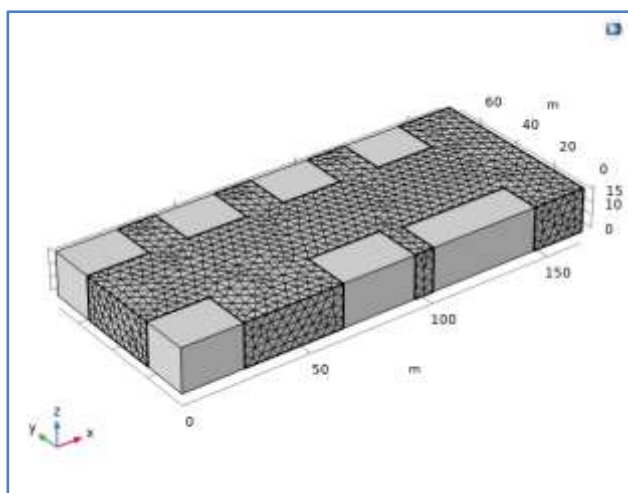


Fig. 4: Mesh of the urban canyon geometry

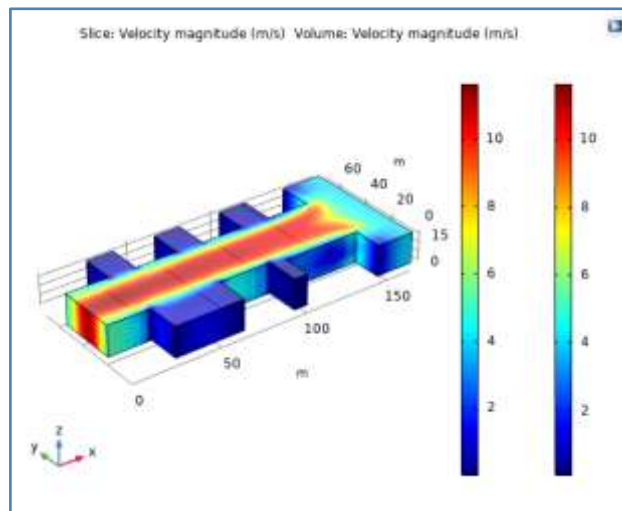


Fig. 5: Benzene gas flow velocity

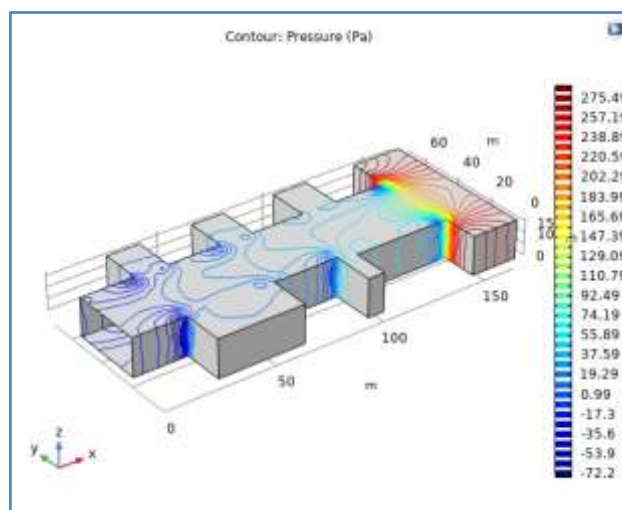


Fig. 6: Pressure distribution in the Urban Canyon

## 5 Conclusion

This study represents the first assessment of ethylene, benzene, and toluene concentrations in the city of Magurele, Romania. These gas air pollutants were measured during the spring and summer seasons, spanning from March to August 2021, at a height of 1.5 meters above the ground. Relationships between the concentrations of these compounds, criteria air pollutants, and meteorological variables were explored across both seasons using a multicomponent detector based on LPAS.

The gas concentrations observed in the environment were found to be influenced by meteorological variables and exhibited seasonal trends. Higher concentrations of these gases were typically recorded during the summer season, particularly on days with elevated temperatures. Wind speed and direction were identified as

significant parameters influencing gas concentrations, with airflow from industrial areas and heavily trafficked roads contributing to increased gas levels. Regarding benzene and toluene, the highest concentrations were observed at points situated within the city and in industrial areas compared to the levels detected in areas surrounded by trees. Ethylene exhibited higher values across all three sampling points, attributed to its involvement in plant physiology. Vehicles and industries emerged as important sources of VOCs. The T/B ratio was utilized to identify these sources, revealing higher values during the spring and summer seasons, indicative of traffic and industrial emissions as predominant contributors. To gain a comprehensive understanding of the behavior of polluting gases in the ambient air, gas concentrations will be determined during both autumn and winter seasons. This approach aims to provide a holistic overview spanning an entire year.

Furthermore, this paper presents a preliminary 3D simulation of benzene gas dispersion within street canyons using Comsol Multiphysics numerical modeling, governed by the RANS equations of compressible turbulent airflow. When performing simulations using the RANS equations in COMSOL Multiphysics or any other CFD software, several types of errors or sources of discrepancy may arise. These errors stem from the discretization of the governing equations and the solution of the resulting algebraic equations using numerical methods. Numerical errors can arise from improper mesh resolution, inadequate numerical schemes, and convergence issues. The RANS equations rely on several assumptions and simplifications, such as the turbulence closure model, boundary conditions, and neglecting certain physical effects (e.g., compressibility effects in incompressible flow simulations). Incorrect specification of boundary conditions, such as inlet velocity profiles, pressure conditions, and wall treatments, can lead to errors in the simulation results. Some errors can come from the quality of the mesh, including element shape, aspect ratio, and mesh density, which can significantly impact the accuracy of the simulation. Poorly structured meshes or insufficient mesh refinement in critical regions can lead to errors. To mitigate these errors, it is essential to conduct thorough verification and validation studies, refine the mesh appropriately, select suitable turbulence models and boundary conditions, and carefully tune solver settings to ensure convergence and accuracy of the simulation results.

In the future, numerical simulations are needed with the modification of the parameters related to the boundary conditions and the size of the mesh.

#### References:

- [1] P. Sicard, E. Agathokleous, A. De Marco, E. Paoletti, V. Calatayud, Urban population exposure to air pollution in Europe over the last decades, *Environ Sci Eur*, Vol. 33, Article number: 28, 2021, <https://doi.org/10.1186/s12302-020-00450-2>.
- [2] L. Liang, P. Gong, Urban and air pollution: a multi-city study of long-term effects of urban landscape patterns on air quality trends, *Sci. Rep.*, Vol. 10, Article no: 18618, 2020, <https://doi.org/10.1038/s41598-020-74524-9>.
- [3] B. Sun, C. Fang, X. Liao, X. Guo, Z. Liu, The relationship between urbanization and air pollution affected by intercity factor mobility: A case of the Yangtze River Delta region, *Environmental Impact Assessment Review*, Vol. 100, Article no. 107092, 2023.
- [4] I. Manisalidis, E. Stavropoulou, A. Stavropoulos, E. Bezirtzoglou, Environmental and Health Impacts of Air Pollution: A Review, *Front Public Health*, Vol. 8, No. 14, 2020, doi: 10.3389/fpubh.2020.00014.
- [5] J. Liang, L. Zeng, S. Zhou, X. Wang, J. Hua, X. Zhang, Z. Gu, L. He, Combined Effects of Photochemical Processes, Pollutant Sources and Urban Configuration on Photochemical Pollutant Concentrations, *Sustainability*, Vol. 15, 2023, Article no. 3281, <https://doi.org/10.3390/su15043281>.
- [6] L. Ehrnsperger, O. Klemm, Air pollution in an urban street canyon: Novel insights from highly resolved traffic information and meteorology, *Atmospheric Environment*, Vol. 13, 2022, Article no. 100151, <https://doi.org/10.1016/j.aeaoa.2022.100151>.
- [7] S. Palzer, Photoacoustic-Based Gas Sensing: A Review, *Sensors*, Vol. 20, No. 9, 2020, Article no. 2745, <https://doi.org/10.3390/s20092745>.
- [8] M. Petrus, C. Popa, A-M Bratu. Determination of Ozone Concentration Levels in Urban Environments Using a Laser Spectroscopy System, *Environments*, Vol. 11, No. 1, 2024.
- [9] M. Cai, Y. Ren, R.G. Gibilisco, B. Grosselin, M.R. McGillen, C. Xue, A. Mellouki, V. Daële, Ambient BTEX Concentrations during the COVID-19 Lockdown in a Peri-Urban Environment (Orléans, France), *Atmosphere*,

Vol. 13, No. 10, 2022,  
<https://doi.org/10.3390/atmos13010010>.

- [10] L. Kong, T. Luo, X. Jiang, S. Zhou, G. Huang, D. Chen, Y. Lan, F. Yang, Seasonal Variation Characteristics of VOCs and Their Influences on Secondary Pollutants in Yibin, Southwest China, *Atmosphere*, Vol. 13, No. 9, 2022, Article no. 1389, <https://doi.org/10.3390/atmos13091389>.
- [11] D. Guo, P. Zhao, R. Wang, R. Yao, J. Hu, Numerical simulations of the flow field and pollutant dispersion in an idealized urban area under different atmospheric stability conditions, *Process Safety and Environmental Protection*, Vol. 136, 2020, pp. 310-323.
- [12] L. P.S. Cruz, D. F. Santos, I. F. dos Santos, Í.V.S. Gomes, A.V.S. Santos, K.S.P.P. Souza, Exploratory analysis of the atmospheric levels of BTEX, criteria air pollutants, and meteorological parameters in a tropical urban area in Northeastern Brazil, *Microchemical Journal*, Vol. 152, 2020, Article no. 104265, <https://doi.org/10.1016/j.microc.2019.104265>.
- [13] Z.M. Malikov, M.E. Madaliev, S.L. Chernyshev, A.A. Ionov, Validation of a two-fluid turbulence model in comsol multiphysics for the problem of flow around aerodynamic profiles. *Sci Rep*, Vol. 14, 2024, Article no. 2306, <https://doi.org/10.1038/s41598-024-52673-5>.
- [14] X. Zheng, H. Montazeri, B. Blocken, Large-eddy simulation of pollutant dispersion in generic urban street canyons: Guidelines for domain size, *Journal of Wind Engineering & Industrial Aerodynamics*, Vol. 211, 2021, Article no. 104527, <https://doi.org/10.1016/j.jweia.2021.104527>.

### **Contribution of Individual Authors to the Creation of a Scientific Article (Ghostwriting Policy)**

- Mioara Petrus carried out the conceptualization, data curation, simulation, and optimization.
- Cristina Popa has executed the spectroscopic experiments, methodology.
- Ana-Maria Bratu has executed the spectroscopic experiments and methodology.

### **Sources of Funding for Research Presented in a Scientific Article or Scientific Article Itself**

This research was funded by a grant from the Ministry of Research, Innovation, and Digitization, CNCS-UEFISCDI, project TE 82/2022, number PN-III-P1-1.1-TE-2021-0717, within PNCDI III.

### **Conflict of Interest**

The authors have no conflicts of interest to declare.

### **Creative Commons Attribution License 4.0 (Attribution 4.0 International, CC BY 4.0)**

This article is published under the terms of the Creative Commons Attribution License 4.0

[https://creativecommons.org/licenses/by/4.0/deed.en\\_US](https://creativecommons.org/licenses/by/4.0/deed.en_US)